Aberrations in Confocal Spectroscopy of Polymeric Materials: Erroneous Thicknesses and Intensities, and Loss of Resolution

STEPHEN MICHIELSEN

Polymer Education and Research Center, School of Textile and Fiber Engineering, Georgia Institute of Technology, Atlanta, Georgia 30332

Received 3 June 2000; accepted 9 October 2000

ABSTRACT: Confocal fluorescence and Raman microscopy are becoming important characterization methods in polymers, especially for blends and films. However, caution must be used in analyzing the data because of the spherical aberration introduced into the illumination and collection of light caused by a mismatch in the indices of refraction of the sample and the design of the microscope objective. In many cases, the measured shape of the region under examination and the measured intensities are rendered invalid because of this aberration. Simultaneously, the axial resolution is degraded because the central light rays and the extreme rays have different focal points. It is shown that the loss of axial resolution can be minimized and the loss in intensity can be either reduced or accounted for. The error in location within the sample and, hence, the shape can be easily corrected. © 2001 John Wiley & Sons, Inc. J Appl Polym Sci 81: 1662–1669, 2001

Key words: confocal microscopy; Raman microscopy; polymers; aberrations; LSCM

INTRODUCTION

Confocal fluorescence and confocal Raman microscopy have been used effectively to analyze the structure of biological systems.[1–3] Using confocal microscopy, it is possible to determine both the structure and the location of structures within a sample without the need to physically section the material. Recently, these techniques have been applied widely to determine the morphology of polymer blends in three-dimensional (3-D) space[4–7]; to characterize films,[7–9] gels,[10] and latex particles[5,7]; and to measure dye diffusion.[11] For example, Hirokawa et al.[10] used laser scanning confocal microscopy (LSCM) to determine the internal structures of poly(*N*-propylacrylamide) gels without the need to physically section the gels. Schrof et al.[7] used confocal fluorescence microscopy to determine the contents of multihollow latex particles, dispersions of polybutadiene copolymers in asphalt, and the morphology of polyamide/poly(phenylene ether) blends. They used confocal Raman microscopy to determine the extent of cure in a radiation-cured polyetheracrylate and the distribution of glass fibers and of $Mg(OH)_2$ flame-retardant particles in a polyamide extrudate. Ling et al.[9] used confocal microscopy to determine the thickness of a poly(2-vinylpyridine) coating on steel. Song et al.[11] used LSCM to measure the concentration of fluorescein in nylon fibers, to determine the diffusion coefficient. A quick search of the literature provides over 200 references to the use of confocal microscopy on polymeric systems. Because the spatial resolution of a confocal fluorescence or confocal

Journal of Applied Polymer Science, Vol. 81, 1662–1669 (2001)

Raman microscope can be as high as about 0.5 μm in all three dimensions, it is anticipated that the use of these techniques will continue to grow rapidly in polymer science because of the rich information it can provide and the ease of sample preparation.

In a typical confocal microscope an illumination source, almost always a laser, is passed through a pinhole. The light coming through this pinhole is imaged via the microscope optics into a focal spot within the sample. The size of this spot is often close to the diffraction limit. The fluorescent or scattered light emanating from the sample is collected and focused onto another pinhole that is placed such that the image of the focal spot falls exactly onto this pinhole. Hence, the illumination pinhole and the imaging pinhole are confocal to each other. The high *x,y,z*-spatial resolution of the confocal microscope arises from the discrimination offered by the imaging pinhole. In an ideal confocal microscope, only a small region in the *x,y*-plane is illuminated. Thus, neither fluorescence nor Raman scattered light can be excited in the object plane, but outside of the focal spot. Even if scattering of the incident beam is sufficient to excite fluorescence outside of the focal point, this light is focused onto the same plane as that of the imaging pinhole, but outside of the pinhole. Thus, it is blocked from reaching the detector. Any fluorescent or scattered light emanating from above or below the focal spot is focused below or above the pinhole, respectively. Because it is out of focus at the image pinhole, the light will be spread over a region larger than the pinhole, and a large fraction of the light will be blocked by the pinhole. On the other hand, any fluorescent or scattered light emanating from the focal spot will be imaged exactly in focus and exactly overlapping the pinhole, thus passing through unimpeded. By scanning the specimen in the *x,y,z*-directions, therefore, a 3-D map of the structure of the material can be made without the need to section the sample.

However, a major limitation to the use of confocal microscopy is often not recognized in the polymer literature. Hell et al.[12] showed that the axial position (z) is in error and the axial resolution of confocal microscopy (CM) is reduced when the refractive index of the sample differs significantly from that of the design of the microscope objective, the design index. The mismatch in refractive indices causes a shift in the focal point. This results in errors in the location, shape, and size of the very structures that one is trying to measure. Furthermore, the mismatch in refractive indices also induces a large spherical aberration that results in a loss in axial resolution and diminishes the fluorescent or Raman scattered intensity. In biological samples this problem is often overcome by using water-immersion objectives, because many of their samples have refractive indices close to 1.33. Unfortunately, this approach has limited application in polymers. The purpose of this study is to point out these effects and to demonstrate the importance of considering them in the interpretation of CM data obtained from polymeric systems.

There are only three common objective types: an air objective (design index of 1.0), a water-immersion objective (design index of 1.33), and an oil-immersion objective (design index of 1.515). Unfortunately, in polymers a convenient match of the refractive indices does not generally occur. For example, the isotropic index of refraction of nylon 6,6 is approximately 1.53, 1.58 for poly(ethylene terephthalate), and 1.49 for polypropylene. The refractive index of each of these polymers differs significantly from that of the oil-immersion objective, 1.515. For oriented films and fibers, the refractive indices are different for different polarizations and along different directions in the fiber or film. The impact of these differences is shown below. They can have a severe effect on the axial resolution of the confocal microscope and lead to apparent errors in the location, size, and shape of the sampling region. Some of these errors can easily be corrected by mathematical manipulation, others cannot. In addition, these effects can cause a severe degradation in the signal and a smearing of the focal point. Thus, great care needs to be taken in analyzing confocal data from polymers.

THEORY AND MEASUREMENT

Hell et al.[12] provided the theory for confocal microscopy of materials whose index differs from that of the design index of the microscope objective. They examined both the imaging of a point source within a medium, whose refractive index differs from the design index of the objective, and the effect this has on the detected light. They showed that there is both a shift in the focal position and a smearing of the image as the refractive-index mismatch increases and as the depth of the original focal depth within the sample increases. For a fixed refractive-index mis-

match and fixed focal depth, the smearing increases as the numerical aperture (*NA*) of the objective increases. These two factors lead to an error in the apparent location of a structure, a loss of axial resolution, and loss of the apparent intensity for high *NA* objectives and large refractive-index mismatches. Even for small differences in the refractive index, the errors can be significant. This investigation provides a geometric optics approach to approximate the distortion of the excitation beam resulting from the refractive-index mismatch between the design of the objective and the realities of the sample. This approach also provides a means to easily correct the data or to reduce the effect by careful choice of experimental conditions.

Axial Positional Errors

Figure 1(b) shows the common focal point for both a near-axis ray and a ray at the maximum angle limited by the *NA* of the objective. Light comes from above in parallel rays and is focused onto the optic axis (OA) by the microscope objective at the working distance *WD*. In this case, all rays originating at the source pinhole have a common focal point. The light emitted or scattered from this focal point is imaged onto the confocal pinhole in the image plane. This pinhole rejects light scattered or emitted from regions above and below the focal plane. It also blocks any light scattered or emitted from points in the focal plane but that lie outside of the focal point. Figure 1(a) shows the same rays for the case in which the sample has a refractive index less than the design index of the objective; Figure 1(c) shows the case in which the sample index is greater than the design index of the objective. In both cases, as the light enters the sample, the rays bend according to Snell's law. The rays near the optic axis of the objective are bent to a different degree than those at large angles to the optic axis. [The original direction of the rays is shown by the dashed-line extensions from the rays in the index-matching oil and they converge at the original or nominal focal point (NFP).] The result is that each cone of illumination is bent a different amount and thus has a different focal plane. The extent of this spherical aberration depends only on the *NA* of the objective, the depth within the sample of the NFP, and the ratio of the refractive indices of the sample (n_s) to the design index of the objective (n_o). For simplicity, we will assume the immersion oil has the same refractive index as the design index of the objective, which is the normal practice. The nominal depth within the sample d_s is given by the location of the NFP and can be represented as the working distance of the objective (*WD*) minus the distance from the bottom of the objective to the top of the sample *D*, or $d_s = WD - D$.

As a light ray moves from the immersion oil into the sample, its angle changes according to Snell's law:

$$\theta_s = \sin^{-1}\left(\frac{n_0}{n_s}\sin\,\theta_0\right) \tag{1}$$

where θ_s is the angle the ray takes within the sample and θ_0 is the original angle within the immersion oil. The focal point for this cone of illumination occurs where all the rays for this cone intersect, ideally at the optic axis. If $n_s = n_o$, then $\theta_s = \theta_0$ and the focal point is just the original focal point. If the sample is raised until this original focal point is at a depth d_s within the sample, the point at which the ray enters the sample is a distance a from the optic axis given by (see Fig. 2 for a description of the geometry):

$$a = d_s \tan\,\theta_0 \tag{2}$$

Figure 1 Spherical aberration is caused by the mismatch of the refractive indices of the sample and the design of the microscope objective. The light comes through the objective from above and the light is focused onto the optic axis (OA) of the objective. The working distance *WD* is the distance from the bottom of the objective to the focal plane; *D* is the distance from the bottom of the objective to the top of the sample; n_o is the refractive index of the immersion oil, which is the same as the index for which the objective is designed; n_s is the refractive index of the sample; *t* is the sample thickness; *FE* is the focal error, which is just the distance between the original focal point and the new focal point. Dashed lines show the original paths of the extreme rays, whereas solid lines show the new paths. The difference between these two lines is the focal error. (a) The sample index is less than the oil index, $n_s < n_o$; (b) $n_s = n_o$; (c) $n_s > n_o$.

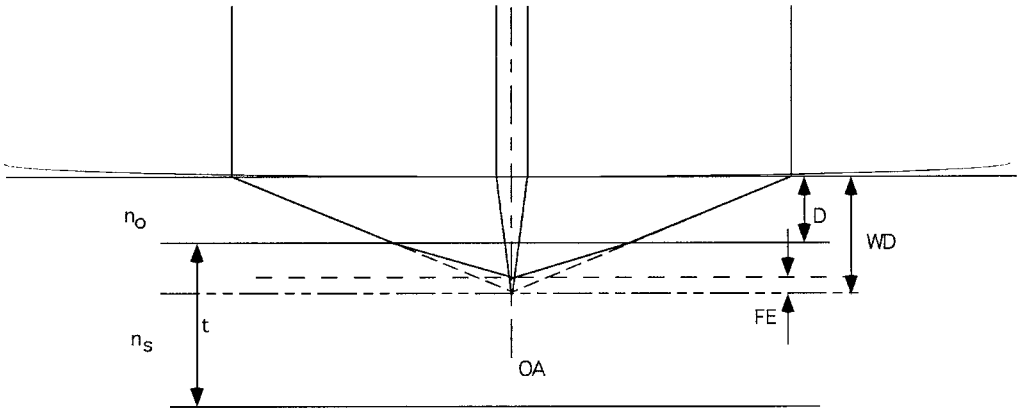

a. $n_s < n_o$

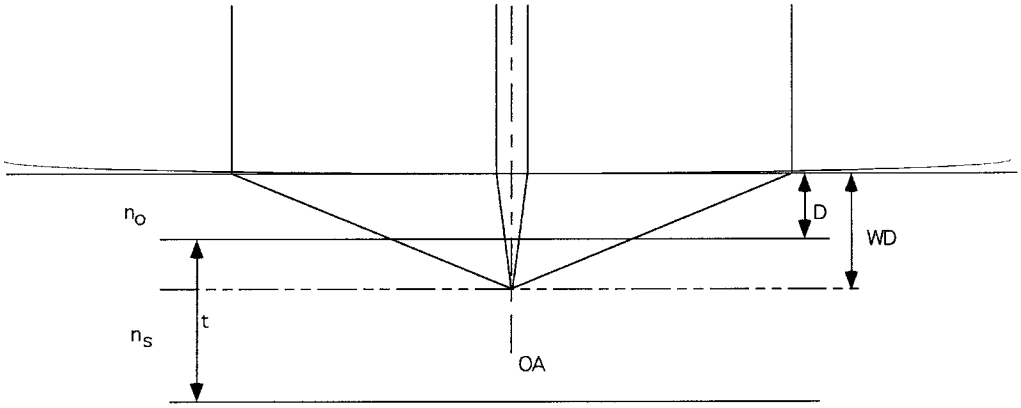

b. $n_s = n_o$

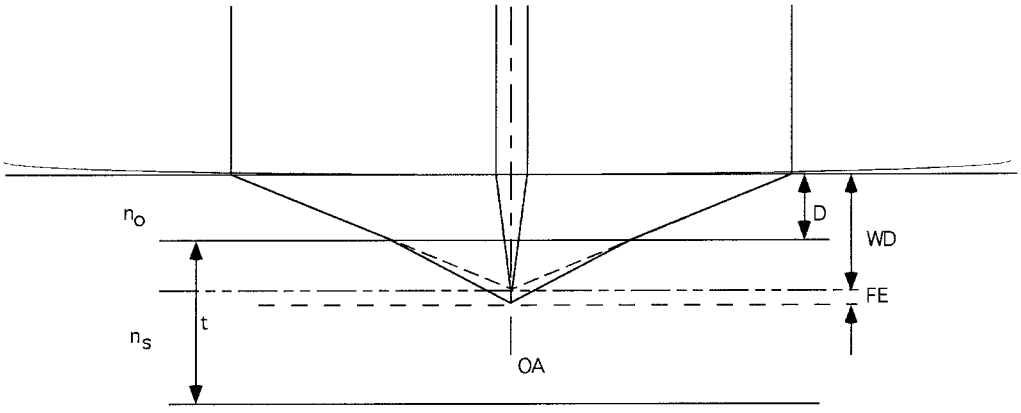

c. $n_s > n_o$

When $n_s \neq n_o$, the focal point shifts as a result of the bending of the rays. The new focal point is

$$f = \frac{a}{\tan \theta_s} = d_s \frac{\tan \theta_0}{\tan \theta_s} \tag{3}$$

Substituting for θ_s and for the tangent function,

$$f = d_s \frac{n_s}{n_0} \frac{\cos\left[\sin^{-1}\left(\frac{n_0}{n_s} \sin \theta_0\right)\right]}{\cos \theta_0} \tag{4}$$

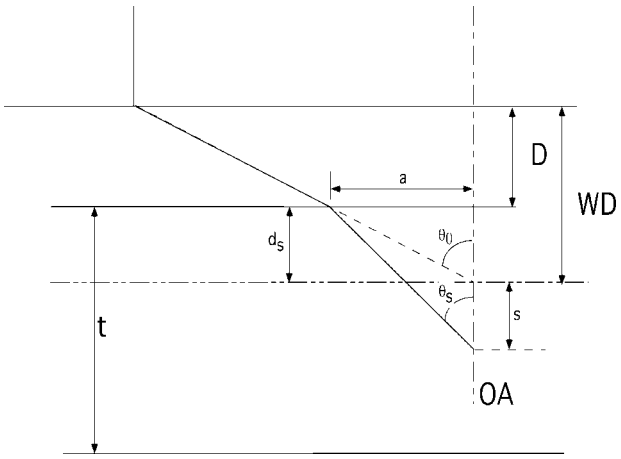

Figure 2 The geometric definitions used for the derivations are shown. OA is the optic axis of the objective; *WD* is the working distance; *D* is the distance from the bottom of the objective to the top of the sample; t is the sample thickness; d_s is the distance from the top of the sample to where the focal plane would be in the absence of the sample; a is the distance from OA to where the light ray enters the sample; θ_0 and θ_s are the angles that the original light ray and the bent light ray make with OA, respectively; s is the shift in the focal point.

At small angles, the shift in focus is approximately

$$f \cong \frac{n_s}{n_0} d_s \tag{5}$$

or

$$d_{\text{real}} \cong \frac{n_s}{n_0} d_{CM} \tag{6}$$

where d_{real} is the real position of the object and d_{CM} is the nominal position determined by confocal microscopy. This position error in the confocal imaging for small *NA* objectives depends only on the ratio of the refractive indices. For example, for an oil-immersion objective with *NA* of 0.5, and $1.0 < n_s < 2.0$, eq. (5) is accurate to within 2%.

The impact of this shift in focus can readily be seen. Ling et al.[9] measured the thickness of a poly(2-vinylpyridine) (PVP) coating on steel using confocal microscopy. They measured a thickness of 5.2 μm using CM, although they calculated a thickness of 8.8 μm based on the measured weight gain of the sample during polymerization and the reported density of 1.153 g/mL. PVP has a refractive index of 1.622,[13] whereas the design index of their objective was 1.0. From eq. (6), the corrected depth is 8.4 μm, in good agreement with the weight gain and the density of bulk polymerized PVP.

Loss of Axial Resolution

To achieve high axial resolution, most confocal microscopes use large *NA* objectives, 0.95 for dry or air objectives and 1.2–1.4 for oil-immersion objectives. In this case, eq. (4) must be used. It indicates that each cone of illumination and each cone of light emitted by the sample has its own focal point. In a well-designed microscope objective used under the design conditions, all focal points will be the same. This is not the case when the sample has a refractive index different from the design index. The spread in the focus s can be defined as the difference in the focal position of the central rays (at angle θ_0) and the extreme rays (at angle θ_e) as limited by the numerical aperture of the objective. Thus,

$$s = d_s \frac{n_s}{n_0} \left| \frac{\cos\left[\sin^{-1}\left(\frac{n_0}{n_s}\sin\theta_c\right)\right]}{\cos\theta_c} - \frac{\cos\left[\sin^{-1}\left(\frac{n_0}{n_s}\sin\theta_e\right)\right]}{\cos\theta_e} \right| \tag{7}$$

where the θ_e is

$$\theta_e = \sin^{-1}\frac{NA}{n_0} \tag{8}$$

or

$$s = d_s \frac{n_s}{n_0} \left| 1 - \frac{\cos\left[\sin^{-1}\left(\frac{NA}{n_s}\right)\right]}{\cos\left[\sin^{-1}\left(\frac{NA}{n_0}\right)\right]} \right| \tag{9}$$

Figure 3 shows how the focus shifts as a function of angle when $n_s = 1.58$, $n_o = 1.515$ ($n_s/n_o = 1.04$, oil immersion), and $d_s = 10$ μm, and for $n_o = 1.0$ (dry objective). All the angles shown lie within the cone of acceptance of a 1.4 *NA* oil-immersion objective and a 0.95 *NA* dry objective, typical of those used in confocal microscopy. This leads to a large spread of the focal point, or a smearing of the focus as well as an offset from

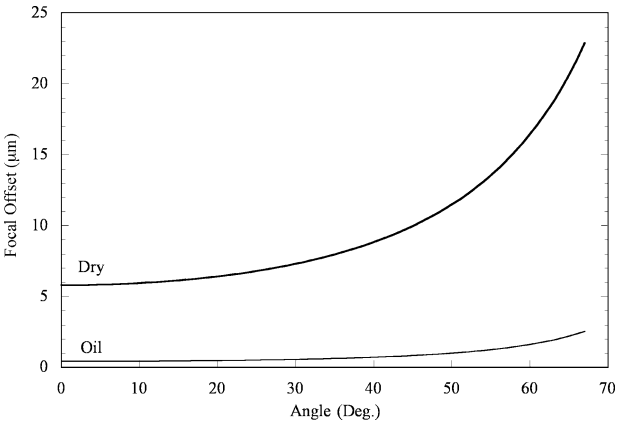

Figure 3 The focal point offset from the nominal focal point is shown for a dry (air) and oil-immersion objective for a polymer with $n_s = 1.58$, and a nominal focal point located 10 μm below the surface (i.e., $d_s = 10$ μm). The focal spread is the difference between the focal offset at 0° and at the maximum angle allowed by the numerical aperture (*NA*) of the objective.

the original focus. In this case, when the NFP is 10 μm, the focal "point" is spread out over a range of 2 μm in the z-direction for the oil-immersion objective and more than 15 μm for the dry objective. In other words, even a very small mismatch in the refractive indices can lead to a large spread in the focal point when using high *NA* objectives. With a large mismatch, the focal spread can be larger than the image depth within the sample. Figure 3 also shows that there is a large shift of the real focal point from the NFP. For the dry objective, the shift at low illumination and collection angles is 6 μm when the NFP is 10 μm below the surface; that is, the location of the focal point is in error by 60%, even for very small *NA* objectives.

The focal spread causes an additional complication. The emitted or scattered light needs to be focused on the imaging pinhole. Each cone of illumination lying between angles θ and $\theta + d\theta$ has its own focal point. Only light emitted or scattered from this focal point within the angles θ and $\theta + d\theta$ will be focused onto the imaging pinhole. The remainder of the light emitted or scattered from this point will be blocked by the pinhole. In other words, the emitted or scattered light originating from the focal point of small illumination angles (i.e., close to the optic axis) will be collected efficiently only at small collection angles, and not at wide angles. Likewise, the emitted or scattered light originating from the focal point of wide illumination angles (i.e., the extreme angles) will be collected efficiently only at wide collection angles. The result of this effect is the loss of z-axis resolution and loss of collection efficiency and thus of detected intensity.

Figure 4 shows the Raman scattered intensity of the 1616 cm^{-1} band of poly(ethylene terephthalate) as a function of the nominal sampling depth within the sample. The film thickness is 2 mil (50.8 μm). The confocal resolution can be estimated from the rise in the signal intensity on entering the film. The distance over which the signal rises from 0 to 100% of the maximum intensity is 2.9 μm on the first side of the film, which is the axial resolution of this microscope. On the second surface, where the depth is 50.8 μm, the distance is 13.4 μm. The expected focal spread for the back surface [according to eq. (9)] is 11 μm, in good agreement with the observed drop-off in intensity on the back surface; that is, as expected, the axial resolution on the backside of the film is substantially less than that on the front surface because of the refractive-index mismatch. Furthermore, the intensity of the 1616 cm^{-1} band drops by 40% in going from the first surface to the second, in agreement with the preceding discussion. Hell et al.[12] showed that this behavior is the result of the refractive-index mismatch and can be fit quantitatively. Finally, the width of this sample, measured between the half-heights on each side of the film, is 48.3 μm. Esti-

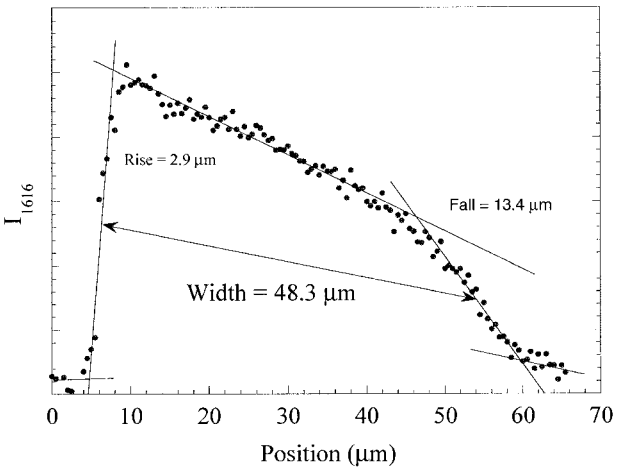

Figure 4 Raman intensity for the 1616 cm^{-1} band of PET for a 2-mil (50.8-μm) thick film using a ×100 oil-immersion objective. Oil is applied only to the top surface; the back surface is dry. Confocal Raman microscopy scans were performed on a Holoprobe Research 785 Raman microscope (Kaiser Optical Systems, Inc.). Axial steps were 0.5 μm.

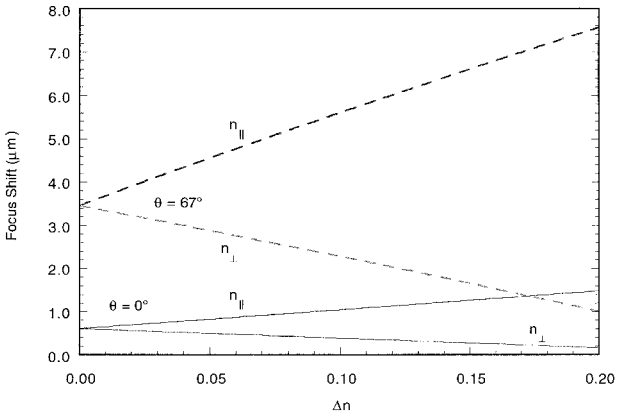

Figure 5 The shift of the focal point is shown as a function of birefringence for $n_{iso} = 1.606$, $d_s = 10$ μm, and $NA = 1.4$.

mating the refractive index of PET as 1.6, the real thickness calculated by way of eq. (6) is 51 μm, a good match with the known thickness. Clearly, these problems are readily accounted for by a proper treatment of both the optics of the sample and the CM optics, thus leading to potential solutions.

In principle, the problems discussed earlier can be alleviated. A judicious choice of an immersion oil with a refractive index that lies on the opposite side of the design index of the microscope objective from the specimen's refractive index could be used to correct for the induced spherical aberration for a single focal plane. Although this approach is not generally useful, because different oils would be needed for each position within the specimen, it is useful for examining a small region within the sample. Another approach is to use microscope objectives optimized for each (isotropic) polymer. The cost would be prohibitive. Perhaps the best solution is to reduce the *NA* of the objective. Although the axial resolution will be degraded, the loss in intensity and the focal spread are reduced[12] and it is possible to calculate the optimum *NA* for the sample.

In oriented films and fibers, the refractive index is frequently anisotropic. In this case, the focus shift and the focus error depend on the polarization of the incident illumination, the polarization of the emitted or scattered light, and the orientation of the sample. Figure 5 shows this effect for polyester fibers with $n_{iso} = 1.606$ and birefringence, $0 \leq \Delta n \leq 0.20$. When $d_s = 10$ μm in this fiber, and for $\Delta n = 0$, the focus shift for a small angle is 0.6 μm and is the same for both polarizations. The focal spread is 2.9 μm for $NA = 1.4$. For a birefringence $\Delta n = 0.2$, the light polarized perpendicular to the fiber axis has a focus shift at small angles of only 0.2 μm; light polarized parallel to the fiber axis has a focus shift at small angles of 1.5 μm. The focus spread for the perpendicularly polarized light is only 0.8 μm, but more than 6 μm for the parallel polarized light. Clearly, if nonpolarized light is used to examine this fiber, the situation is even more complex. Confocal microscopy of oriented fibers and films requires the appropriate choice of the polarization of the incident and scattered light to minimize the effects of refractive-index mismatch.

CONCLUSIONS

Confocal microscopy of polymers can be a very useful tool for determining the morphology of polymer blends, thicknesses of laminates, depth profiling of the curing of polymers, and so forth. However, caution must be exercised in the interpretation of the data because of errors introduced by the mismatch of the refractive index of the sample and of the microscope objective. Dry objectives should be used to measure only the surface profile of the surface on which the light is incident. Water-immersion objectives should be used when the sample has an index close to that of water, such as in a highly swollen hydrogel or in biological samples. In all other cases, oil-immersion objectives of appropriate numerical aperture should be used. When possible, the structures of interest should be as close as possible to the incident surface, to minimize these effects. In all cases, the above-discussed issues should be explicitly considered in the interpretation of the confocal data.

REFERENCES

1. Lansing, T. D.; Wang, Y.-L., Eds. Fluorescence Microscopy of Living Cells in Culture; Academic Press: New York, 1989.
2. Pawley, J. B., Ed. Handbook of Biological Confocal Microscopy; Plenum Press: New York, 1995.
3. Paddock, S. W., Ed. Confocal Microscopy Methods and Protocols; Humana Press: Clifton, NJ, 1999.

4. Verhoogh, H.; van Dam, J.; Posthuma de Boer, A.; Draaijer, A.; Houpt, P. M. Polymer 1993, 34, 1325.
5. Markwart, L.; Kip, B. J Appl Polym Sci 1996, 61, 231.
6. Markwart, L.; Kip, B.; Da Silva, E.; Roussel, B. Appl Spectrosc 1995, 49, 1411.
7. Schrof, W.; Klinger, J.; Heckmann, W.; Horn, D. Colloid Polym Sci 1998, 276, 577.
8. Saçak, M.; Akbulut, U.; Batchelder, D. N. Polymer 1998, 39, 4735.
9. Ling, X.; Pritzker, M. D.; Byerley, J. J.; Burns, C. M. J Appl Polym Sci 1998, 67, 149.
10. Hirokawa, Y.; Jinnai, H.; Nishikawa, Y.; Okamoto, T.; Hashimoto, T. Macromolecules 1999, 32, 7093.
11. Song, Y.; Srinivasarao, M.; Tonelli, A.; Balik, C. M.; McGregor, R. Macromolecules 2000, 33, 4478.
12. Hell, S.; Reiner, G.; Cremer, C.; Stelzer, E. H. K. J Microsc 1993, 169(3), 391.
13. Shizuo, A.; Yoshida, M.; Ogawa, Y. Bull Chem Soc Jpn 1975, 48, 1417.